JACS Au
AN OPEN ACCESS JOURNAL OF THE AMERICAN CHEMICAL SOCIETY

pubs.acs.org/jacsau
Letter

Deuterium Metabolic Imaging of the Brain Using 2-Deoxy-2-[$^2H_2$]-D-glucose: A Non-ionizing [^{18}F]FDG Alternative

Xiao Gao, Kai Qiao, David M. Wilson,* Myriam M. Chaumeil,* and Jeremy W. Gordon*

Cite This: *JACS Au* 2025, 5, 571−577
Read Online

ACCESS | Metrics & More | Article Recommendations | Supporting Information

ABSTRACT: The positron emission tomography (PET) tracer 2-deoxy-2-[^{18}F]fluoroglucose ([^{18}F]FDG) is widely used to study diseases where glucose metabolism is dysregulated, including cancer and neurodegenerative disorders. Here we investigate the hypothesis that the 2-position deuterium-enriched analogue 2-deoxy-2-[$^2H_2$]-D-glucose (2-DG-d2) can also map glucose uptake using deuterium metabolic imaging (DMI) without ionizing radiation. To accomplish this, we used a spectrally selective multiband radiofrequency pulse and balanced steady-state free procession (bSSFP) technique, enabling rapid ^{2}H imaging with high specificity and sensitivity to 2-DG-d2. Both *in vitro* and *in vivo* validations demonstrated the sequence's ability to suppress endogenous water signal. Mapping of 2-DG-d2 with high spatial resolution was achieved in healthy mouse brains, comparable to what might be obtained using [^{18}F]FDG PET. The numerous applications of [^{18}F]FDG PET, as well as recent clinical translation of the natural abundance 2-deoxy-D-glucose (2-DG) parent sugar, suggest that DMI using 2-DG-d2 may be applied to patients in the future.

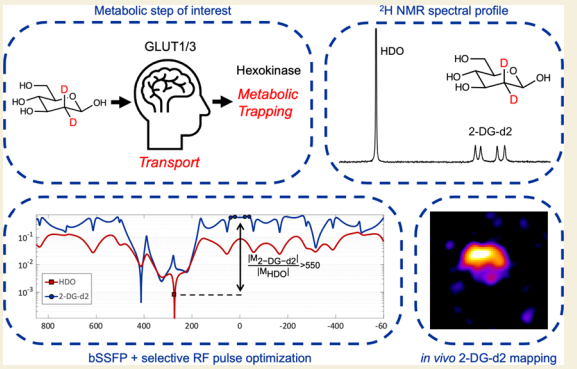

KEYWORDS: *deuterium metabolic imaging, 2-deoxy-2-[$^2H_2$]-D-glucose, glucose, metabolism, FDG*

Positron emission tomography (PET) using 2-deoxy-2-[^{18}F]fluoroglucose ([^{18}F]FDG) has proven to be a powerful tool in different oncological and non-oncological scenarios, e.g., precise localization of tumors,[1] differential diagnosis of neurodegenerative dementias,[2] and detection of vascular inflammation.[3] [^{18}F]FDG shares a similar metabolic fate as glucose except for its 2-position fluorination leading to metabolic arrest (Figure 1A). [^{18}F]FDG is transported intracellularly via glucose transporters and is phosphorylated by hexokinase (*EC 2.7.1.1*). The phosphorylated adduct lacks the 2-position hydroxyl group, making it unable to undergo further conversion to the corresponding fructose derivative that is essential in the glycolysis pathway. With being arrested at the early stage of glycolysis, [^{18}F]FDG retention can be mapped using PET, revealing changes in glucose uptake.

In this Letter, we exploit an analogous mechanism using 2-deoxy-2-[$^2H_2$]-D-glucose (2-DG-d2) that also lacks the 2-position hydroxyl group, proposed as a new probe for deuterium metabolic imaging (DMI). Like [^{18}F]FDG, 2-DG-d2 is trapped intracellularly after being phosphorylated by hexokinase to give 2-DG-d2-6-phosphate. Furthermore, 2-DG-d2/2-DG-d2-6-phosphate can be imaged via the unique frequencies of the 2-position deuterons in NMR (Figure 1B).

Deuterium (^{2}H) NMR, first developed in the 1960s,[4] has recently gained newfound interest in the form of DMI. A variety of deuterated substrates are under active investigation to target disease-dependent metabolic changes, for example [6,6′-$^2H_2$]glucose in stroke and tumors, [2,3-$^2H_2$]fumarate in lymphoma, [$^2H_7$]glucose in detection of Warburg metabolism, and [6,6′-$^2H_2$]fructose in liver cancer.[5−8]

To date, most DMI methods focus on the conversion of a deuterium-enriched substrate (i.e., [6,6′-$^2H_2$]glucose) to an abundant downstream metabolite (i.e., lactate). An alternate strategy would be the detection of a retained deuterium probe with unique NMR chemical shift, which is possible for 2-DG-d2 because the 2-position deuterons resonate significantly upfield from water. In this study, we combined 2-DG-d2 with an optimized ^{2}H imaging approach, namely, a spectrally selective multiband radiofrequency (RF) pulse and a balanced steady-state free precession (bSSFP) sequence, the latter of which has recently demonstrated excellent sensitivity-enhancing capability in DMI.[9,10] The metabolic trapping of 2-DG-d2 at the early stage of glycolysis leads to limited ^{2}H-enriched metabolites, i.e., water (HDO), 2-DG-d2, and 2-DG-d2-6-phosphate, with an infinitesimal chemical shift difference separating the latter two (Figure S1). The resultant sparse

Received: September 23, 2024
Revised: January 21, 2025
Accepted: January 21, 2025
Published: February 6, 2025

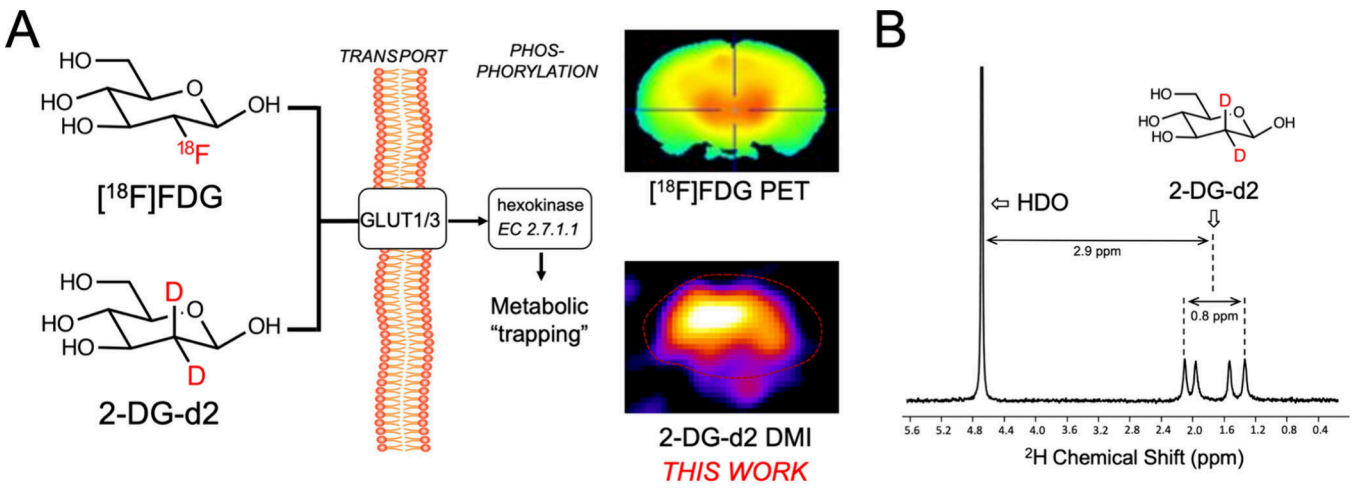

Figure 1. Metabolism and imaging of [^{18}F]FDG and 2-DG-d2. (A) Both the PET tracer [^{18}F]FDG and our new DMI probe 2-DG-d2 are modified at the 2-position and have a presumed mechanism of intracellular retention. The retained [^{18}F] radionuclide can be detected via PET, while unique ^{2}H signals can be detected via DMI. The [^{18}F]FDG PET image of the normal murine brain is reproduced with permission from ref 11. Copyright 2019 Society of Nuclear Medicine and Molecular Imaging. (B) The DMI probe 2-DG-d2 was designed based on the expected chemical shift of 2-position deuterons (2.9 ppm upfield from HDO).

spectral profile offers the potential to develop rapid ^{2}H imaging sequences with high spatial resolution and sensitivity. To optimize rapid 2-DG-d2 imaging, the spectral profile and relaxation times of 2-DG-d2 were first determined. Next, a multiband selective RF pulse was generated to achieve selective 2-DG-d2 excitation and HDO suppression at 14.1 T, followed by bSSFP sequence optimization via a Bloch simulation. Both the specificity and sensitivity of rapid 2-DG-d2 imaging were evaluated on phantoms and animals. An *in vivo* spectroscopy study was also implemented after intraperitoneal (ip) injection to confirm the retention of 2-DG-d2/2-DG-d2-6-phosphate within the healthy mouse brain.

Methods

18.8 T Phantom Study. 2-DG-d2 was custom-synthesized by Sigma-Aldrich ISOTEC. ^{2}H NMR spectroscopy on an 18.8 T Bruker system was implemented to analyze a 30 mM 2-DG-d2 phantom for its chemical shift information.

14.1 T Phantom Study. All NMR experiments at 14.1 T were run on an Agilent system using a 40 mm ^{1}H Agilent volume coil and a 16 mm ^{2}H surface coil from Doty Scientific. A 1 M 2-DG-d2 phantom was analyzed for T_1/T_2 measurements of 2-DG-d2 and HDO at 14.1 T.

The multiband selective RF pulse for 2-DG-d2 imaging was generated using the CVX pulse design toolbox as described previously,[12] using the following input constraints: for 2-DG-d2, central frequency = 0 Hz, bandwidth (BW) = 140 Hz, flip angle (FA) = 90°, ripple = 0.05; for HDO, central frequency = 275 Hz, BW = 130 Hz, FA = 0°, ripple = 0.01.

To evaluate the multiband RF pulse's specificity for 2-DG-d2, 55 M HDO and 100 mM 2-DG-d2 phantoms were tested using an unoptimized 3D bSSFP sequence with either a hard pulse or the generated multiband selective RF pulse. To further improve the sensitivity to 2-DG-d2, the bSSFP sequence underwent optimization via Bloch simulation[13] and was tested on two phantoms containing 10 mM and 100 mM 2-DG-d2, respectively. Using the same experimental setup, a ^{2}H 2D CSI sequence was also implemented to demonstrate the 2-DG-d2 selectivity of the multiband RF pulse compared to a nonselective hard pulse.

14.1 T *In Vivo* Study. All animal research was approved by the Institutional Animal Care and Use Committee of the University of California, San Francisco. For DMI experiments, mice were anesthetized using isoflurane (1.3−1.8% in O_2) and placed in a dedicated cylindrical cradle. An MR setup identical to the phantom studies was used on the 14.1 T scanner. For animal experiments involving 2-DG-d2 administration, ip injection was performed at a dose of 3 g/kg of body weight (dissolved in 500 μL of saline) after a 12 h fast, followed by 30 min of preparation time before the DMI scan. The respiration rate was continuously monitored through the PC-sam software interface (SA Instrument, NY, USA).

Three different ^{2}H NMR experiments were performed on the healthy mouse brain: 2D CSI for multiband RF pulse selectivity validation, nonlocalized spectroscopy to assess the intracerebral dynamics of 2-DG-d2, and 3D bSSFP for 2-DG-d2 mapping. Before each ^{2}H NMR experiment, a ^{1}H fast spin echo sequence was used to acquire T_2-weighted imaging of mouse brain anatomy. The region of interest of ^{2}H CSI and 3D bSSFP was aligned along the brain craniocaudal axis and centered at the level of the hippocampus septal pole.

Data Processing. All ^{2}H NMR spectroscopy data (nonlocalized spectroscopy and 2D CSI) were analyzed using Mnova (Mestrelab Research). The 3D bSSFP data underwent the following postprocessing using VnmrJ (Agilent): 2× zero-filling in the $x-y$ plane and 10 dB Gaussian kernel filtering.

Results

DMI methods generally rely on detecting the production of either deuterium enrichment of water or a metabolite (e.g., lactate) with a chemical shift distinct from water (~4.7 ppm). We therefore designed 2-DG-d2 anticipating that the loss of the 2-position hydroxyl would result in a significant chemical shift off HDO, simplifying the detection of 2-DG-d2 *in vivo*. We first studied a 30 mM 2-DG-d2 phantom using ^{2}H NMR spectroscopy at 18.8 T, which showed two doublets centered ~2.9 ppm upfield of HDO (Figure 1B). The acquired spectral profile demonstrated >2 ppm separation between the HDO and 2-DG-d2 chemical shifts, which facilitated the generation of a multiband selective RF pulse designed to maximize 2-DG-d2 excitation while suppressing the HDO signal. Using

https://doi.org/10.1021/jacsau.4c00888
JACS Au 2025, 5, 571−577

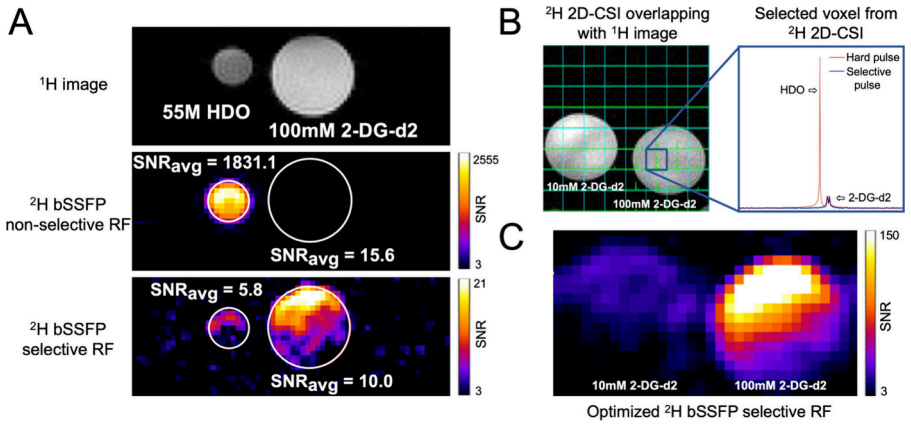

Figure 2. Specificity and sensitivity validation of the proposed 2-DG-d2 imaging strategy using phantom imaging. (A) Phantoms were developed with a large difference in [^{2}H] content (55 M D_2O, small diameter; 100 mM 2-DG-d2, large diameter). Top panel: ^{1}H image of the two phantoms. Bottom two panels: despite the large difference in [^{2}H], using a 3D bSSFP sequence + multiband selective RF pulse reduced the signal to noise ratio (SNR) between HDO and 2-DG-d2 from over 100:1 to less than 1:1 compared to a nonselective RF pulse. (B) 2D-CSI of 10 and 100 mM 2-DG-d2 phantoms. The signal from the HDO portion of the spectrum was suppressed to a below-noise-floor level after switching from the nonselective pulse to the multiband selective RF pulse, while 2-DG-d2 signal was barely influenced. (C) The optimized 3D bSSFP sequence + multiband selective RF pulse was implemented on the same phantom setup as in (B). The proposed imaging strategy is sensitive in capturing the deuterium signal from the 10 mM 2-DG-d2 phantom in less than 12 min.

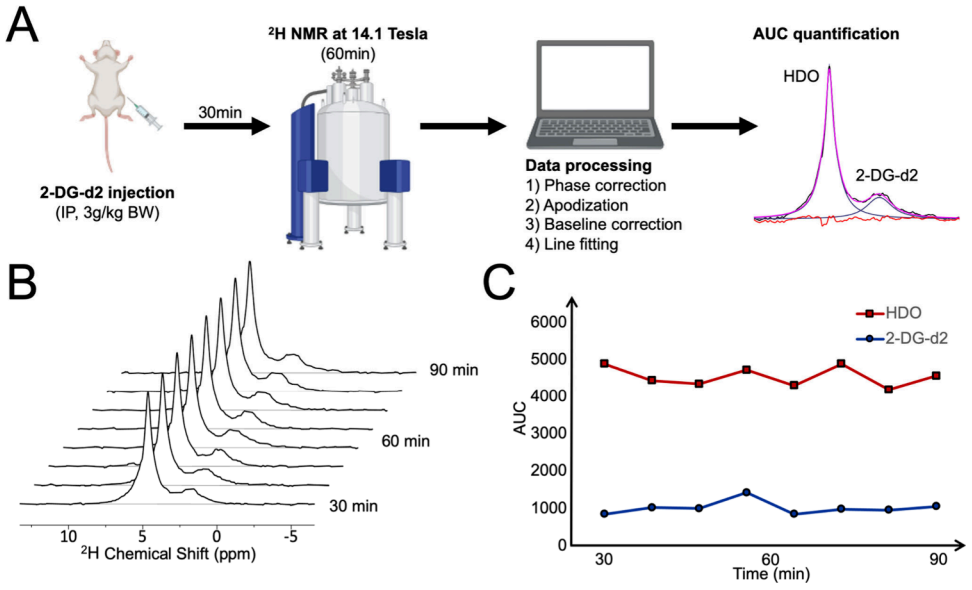

Figure 3. Studying mice after 2-DG-d2 injection. (A) Workflow for dynamic ^{2}H NMR spectroscopy of a healthy mouse brain following 2-DG-d2 administration using a nonlocalized spectroscopy sequence (dynamic acquisition). (B, C) The spectral fitting and AUC quantification results of dynamic ^{2}H NMR spectroscopy showed that the intracranial 2-DG-d2 signal was consistent between 30 and 90 min after 2-DG-d2 ip injection.

frequency separation as a design constraint for the convex optimization (CVX) pulse design toolbox,[12] the shortest pulse had a duration of 5.8 ms and a peak amplitude of 0.47 G (Figure S2A), providing greater HDO suppression than a standard minimum-phase single-band RF pulse (Figure S2B,C). According to the Bloch simulation, the spectral response of the multiband selective RF pulse met our design criteria in fully exciting 2-DG-d2 ($\min_{|Mxy|} > 0.95$) while suppressing HDO ($\max_{|Mxy|} < 0.01$).

Based on the upfield ^{2}H chemical shift of 2-DG-d2, a spectrally selective bSSFP imaging approach to DMI appeared to be feasible for high-resolution frequency-specific brain imaging. Relaxation studies performed at 14.1 T gave an estimated T_1/T_2 of 320 ms/78 ms for HDO and 47 ms/47 ms for 2-DG-d2 (Figure S2D), values that were used for bSSFP parameter optimization. Using a 55 M HDO phantom and a 100 mM 2-DG-d2 phantom, a 3D bSSFP sequence (T_R/T_E = 17 ms/8.5 ms, FA = 90°) was tested along with the generated multiband selective RF pulse (Figure 2A). The following signal to noise ratio (SNR) quantification (see Methods) showed that after switching the RF pulse from a nonselective pulse to a 2-DG-d2 selective pulse, the HDO SNR was reduced by more than 2 orders of magnitude (1831.1 vs 5.8). In contrast, the 2-DG-d2 SNR was similar (15.6 vs 10.0), demonstrating the robust 2-DG-d2 specificity and sensitivity of the proposed DMI strategy.

The specificity and sensitivity of the optimized 2-DG-d2 imaging strategy were subsequently validated via both spectroscopy (2D-CSI) and 3D bSSFP experiments using the 10 mM and 100 mM 2-DG-d2 phantoms at 14.1 T. The 2D-

https://doi.org/10.1021/jacsau.4c00888
JACS Au 2025, 5, 571−577

CSI phantom results once again demonstrated the specificity of the multiband selective RF pulse toward 2-DG-d2 (Figure 2B), where the HDO signal was below the noise floor (SNR < 3) compared to a nonselective hard pulse (selective pulse: SNR_{AUC} = 5.74, SNR = 2.92; hard pulse: SNR_{AUC} = 625.70, SNR = 357.19). To further improve the specificity and sensitivity to 2-DG-d2, Bloch simulations were used to improve the parameters of the bSSFP sequence. This simulation showed that a shorter bSSFP sequence (T_R/T_E = 9 ms/4.5 ms, FA = 60°) combined with the multiband RF pulse resulted in the highest average signal intensity from 2-DG-d2 bandwidth and a further reduction in HDO signal, providing >550-fold suppression of HDO signals (Figure S2B). Using the optimized bSSFP sequence and multiband RF pulse, we could detect signal from a 10 mM 2-DG-d2 phantom within ∼12 min with 1.25 mm × 1.25 mm × 2.5 mm resolution (Figure 2C). These studies indicated the potential detection of 2-DG-d2 and/or phosphorylated 2-DG-d2 *in vivo*.

In preparation for bSSFP imaging, we first studied the normal mouse brain using the 2-DG-d2 selective pulse and 2D CSI. The normal mouse brain was first studied without 2-DG-d2 administration (Figure S3), yielding HDO suppression analogous to the phantom studies. The following SNR analysis showed that HDO was suppressed and barely detected from the ^{2}H spectrum using the multiband selective pulse (selective pulse: SNR_{AUC} = 5.81, SNR = 1.39; hard pulse: SNR_{AUC} = 28.82, SNR = 6.89), indicating that the approach is efficiently selective for 2DG-d2 even in the presence of B_0 field inhomogeneities. After this demonstration of HDO suppression, the intracranial dynamics of 2-DG-d2 was studied following its ip administration (Figure 3A) using nonlocalized NMR spectroscopy, whose result (Figure 3B,C) suggested that brain 2-DG-d2 signals were already at steady state sometime earlier than 30 min after ip injection (3g/kg of body weight) and appeared to be relatively stable in the following 60 min, suggesting the metabolic trapping of 2-DG-d2 *in vivo*.

A DMI glucose administration protocol analogous to that of [^{18}F]FDG PET was sought,[14] whereby a high-resolution image of a metabolically trapped nucleus (^{2}H for DMI, ^{18}F for PET) was acquired at a single time point. For selective detection of the 2-position deuterons of 2-DG-d2, we performed 3D bSSFP 90 min following 2-DG-d2 ip injection into a healthy female mouse. The optimized 3D bSSFP sequence was able to detect the distribution of intracranial 2-DG-d2 and its metabolites using an ∼20 min scan at high spatial resolution (1.25 mm × 1.25 mm × 2.5 mm) (Figure 4A), with the mapping of intracranial 2-DG-d2 at different craniocaudal levels (Figure 4C). In contrast, when the same DMI protocol was applied to an age- and sex-matched animal without 2-DG-d2 injection, signals were below the noise floor (Figure 4B).

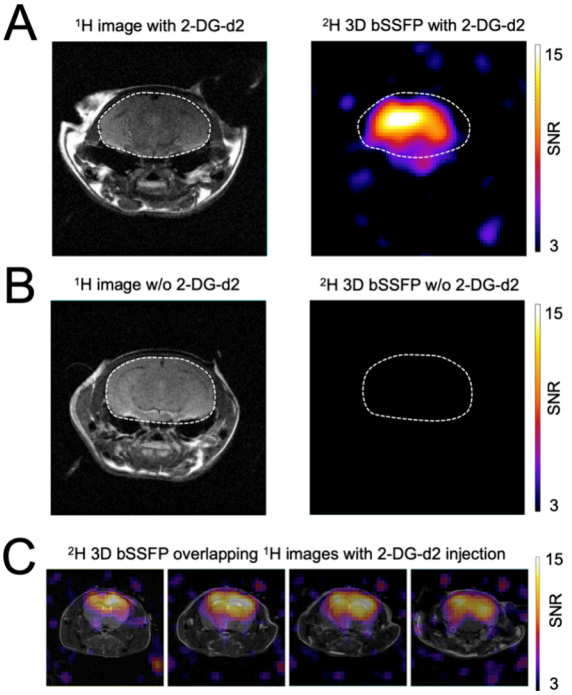

Figure 4. Imaging of 2-DG-d2 in the murine brain using bSSFP. (A) At 90 min after ip injection of 2-DG-d2, 3D bSSFP can detect the distribution of intracranial 2-DG-d2 (and presumably its structurally related metabolites) at a spatial resolution of 1.25 mm × 1.25 mm × 2.5 mm. A ^{1}H MRI image of the brain is highlighted on the left (outlined by a dotted line) with the bSSFP image on the right. (B) When the same scan was applied on a control animal receiving no 2-DG-d2 injection, the imaging signal was below the noise floor. (C) Fused ^{1}H and DMI images are shown to indicate distribution of ^{2}H bSSFP signals from different brain craniocaudal levels.

Discussion

In this study, we showed that DMI could be used to detect 2-DG-d2 and presumably its chemically analogous metabolites (2-DG-d2-6-phosphate) with high spatial resolution in the normal murine brain. This was accomplished via a multiband selective RF pulse and bSSFP sequence. The specificity and sensitivity of the proposed DMI strategy were validated using both phantoms and normal mice. Volumetric imaging of 2-DG-d2 in the healthy mouse brain was achieved with a higher spatial resolution (<4 μL) and shorter scan time (<20 min) versus the 2D CSI sequence (spatial resolution = 8−27 μL, scan time = 30−35 min) reported by [6,6′-$^2H_2$]glucose rodent DMI studies.[15,16] Several innate NMR properties of 2-DG-d2 were also investigated. The near unity T_2/T_1 ratio of 2-DG-d2 made bSSFP-based acquisition an ideal strategy to image 2-DG-d2 due to its high SNR efficiency compared to spoiled-GRE sequences.[17] Furthermore, the most beneficial NMR characteristic of 2-DG-d2 is its large (2.9 ppm) chemical shift from HDO. This is in contrast to other deuterated glucose analogs that were recently reported, such as deuterated 3-*O*-methylglucose (OMG) whose chemical shift is <1.5 ppm from HDO.[18] The larger spectral separation relaxes the multiband RF pulse design constraints, making it easier to achieve sharp stopband (HDO suppression) and passband (2-DG-d2 excitation) while maintaining a short RF pulse duration. Another yet unexplored advantage brought by the sparse ^{2}H spectrum is an HDO image acquired in an analogous manner, as proposed for 2-DG-d2. The resultant HDO mapping can be used as an internal reference and aid in 2-DG-d2 quantification, though it is important to note that the smaller T_2/T_1 ratio of HDO will result in reduced sensitivity using this bSSFP-based approach.

The 2-DG-d2 signal observed in this work was largely localized to the murine brain. This is due in part to the use of a 16 mm surface coil, which provides high-sensitivity coverage over the brain, but the ^{2}H signal is attenuated as the distance from the coil increases. A volume coil would provide deeper tissue coverage at the expense of reduced sensitivity, which would necessitate longer scan times or coarser resolution to regain SNR. In addition, the typical PET-FDG study in a

https://doi.org/10.1021/jacsau.4c00888
JACS Au 2025, 5, 571−577

human has massive brain uptake relative to surrounding structures in the head/neck. Just as tissues other than the brain have low glucose uptake in PET-CT in the head/neck region, in the sensitive region of the ^{2}H coil, we did not observe tissues other than the brain itself.

Although [6,6′-$^2H_2$]glucose, so far the most common DMI probe, can be used to monitor glucose catabolism by detecting the downstream products of glycolysis (lactate and Glx), [^{18}F]FDG PET reveals more proximal events in glycolysis, namely, glucose uptake and subsequent 6-position phosphorylation that leads to trapping of [^{18}F]FDG.[19] The utility of [^{18}F]FDG PET has been demonstrated in extensive patient data in the past decades: increased [^{18}F]FDG uptake is observed in different cancers (an essential feature of the Warburg effect), and decreased [^{18}F]FDG uptake is seen in neurodegenerative conditions like Alzheimer's and Parkinson's diseases.[20] On the contrary, [6,6′-$^2H_2$]glucose DMI cannot precisely provide a measure of glucose uptake, since there is potential loss of ^{2}H labeling to the HDO pool during glucose catabolism, leading to a nonstoichiometric relationship between [6,6′-$^2H_2$]glucose uptake and the downstream metabolite production.[6,21] In contrast, 2-DG-d2 DMI can more directly reflect glucose uptake like [^{18}F]FDG PET and is also featured for being nonradioactive and readily accessible, providing a wider usage in longitudinal studies than [^{18}F]FDG PET.

According to our nonlocalized ^{2}H spectroscopy results, although the intracranial 2-DG-d2 signal was consistent between 30 and 90 min after ip injection, at 22 h postinjection there was barely remaining 2-DG-d2 detected from the mouse brain (Figure S4). Since the conversion between 2-DG and 2-DG-6-phosphate is reversible and the clearance of 2-DG from the vascular bed is rapid, its equilibrium intracellular concentration will be subject to (1) continuous phosphorylation of 2-DG and dephosphorylation of 2-DG-6-phosphate and (2) 2-DG reentering the blood. These two main factors result in a half-life of ∼1.4 h for the total 2-DG/2-DG-6-phosphate pool in the brain,[22] which kinetics should be followed by both [^{18}F]FDG and 2-DG-d2. However, unlike [^{18}F] with a 1.8 h half-life, 2-DG-d2 can provide a more direct inference of the metabolic fate of 2-DG after being taken up by cells.

A significant limitation of the proposed method is the potential toxicity of 2-DG-d2 at the doses required for high-resolution brain imaging. The parent (nonenriched) metabolite 2DG has been studied in several clinical trials, including those treating advanced solid tumors (up to 88 mg kg^{-1} day^{-1})[23] and most recently for COVID-19 (up to 126 mg kg^{-1} day^{-1}).[24,25] 2DG is also well-tolerated in mice ($LD_{50} \geq 8$ g/kg in mice).[16] 2DG has been administered in doses up to 250 mg/kg to treat patients with glioblastoma multiforme without any adverse side effects,[26] which is similar to the mouse dose used in this study, obtained via a standard calculation based on body surface area.[27] Thus, although the antimetabolite characteristics of 2DG are well-known, these quantities suggest the feasibility of patient use after further optimization of the imaging protocol and coil design that leads to lower 2-DG-d2 doses for human imaging. With respect to the general safety of DMI, deuterated molecules have been studied and implemented in humans for many years, especially water itself (D_2O).[28−31] Of note, even the high [6,6′-$^2H_2$]-glucose doses administered to humans[15] merely caused an approximately 0.5−1.5% rise in the total deuterium-enriched body water, significantly below the toxicity threshold (∼20%).[32]

Conclusion

This study shows the feasibility of imaging the normal brain using DMI and the nonradioactive glucose analog 2-DG-d2, which is chemically and biochemically analogous to the PET tracer [^{18}F]FDG. Like [^{18}F]FDG PET, the developed DMI strategy is likely specific for the detection of altered glucose uptake, a biomarker in numerous human diseases. Additional studies will be required to establish the relevance of 2-DG-d2 in disorders for which glucose metabolism is dysregulated, including Alzheimer's disease and cancer. Potential applicability in humans is dependent on both understanding the 2-DG-d2 dose required and the transition to clinically relevant magnetic field strengths.

■ ASSOCIATED CONTENT

Supporting Information

The Supporting Information is available free of charge at https://pubs.acs.org/doi/10.1021/jacsau.4c00888.

Additional experimental details, materials, and methods and supplemental figures (PDF)

■ AUTHOR INFORMATION

Corresponding Authors

David M. Wilson − *Department of Radiology and Biomedical Imaging, University of California San Francisco, San Francisco, California 94158, United States;* orcid.org/0000-0002-1095-046X; Email: david.m.wilson@ucsf.edu

Myriam M. Chaumeil − *Department of Radiology and Biomedical Imaging, Department of Physical Therapy and Rehabilitation Science, and UC Berkeley−UCSF Bioengineering Program, University of California San Francisco, San Francisco, California 94158, United States;* orcid.org/0000-0002-2110-4613; Email: myriam.chaumeil@ucsf.edu

Jeremy W. Gordon − *Department of Radiology and Biomedical Imaging and UC Berkeley−UCSF Bioengineering Program, University of California San Francisco, San Francisco, California 94158, United States;* orcid.org/0000-0003-2760-4886; Email: jeremy.gordon@ucsf.edu

Authors

Xiao Gao − *Department of Radiology and Biomedical Imaging, Department of Physical Therapy and Rehabilitation Science, and UC Berkeley−UCSF Bioengineering Program, University of California San Francisco, San Francisco, California 94158, United States*

Kai Qiao − *Department of Radiology and Biomedical Imaging and Department of Physical Therapy and Rehabilitation Science, University of California San Francisco, San Francisco, California 94158, United States*

Complete contact information is available at: https://pubs.acs.org/10.1021/jacsau.4c00888

Author Contributions

X.G.: methodology, investigation, data curation, formal analysis, visualization, writing—original draft, writing—review and editing. K.Q.: methodology, formal analysis. D.W.: conceptualization, writing—review and editing, funding acquisition. M.M.C.: conceptualization, writing—review and

https://doi.org/10.1021/jacsau.4c00888
JACS Au 2025, 5, 571−577

editing, supervision, funding acquisition. J.G.: conceptualization, methodology, writing—review and editing, supervision, funding acquisition. CRediT: **Xiao Gao** data curation, formal analysis, investigation, methodology, writing - original draft; **Kai Qiao** data curation, formal analysis, methodology; **David M. Wilson** conceptualization, investigation, supervision, validation, visualization, writing - original draft, writing - review & editing; **Myriam Chaumeil** conceptualization, data curation, funding acquisition, investigation, writing - original draft, writing - review & editing; **Jeremy W Gordon** conceptualization, formal analysis, funding acquisition, investigation, methodology, resources, supervision, writing - original draft, writing - review & editing.

Funding

This study was funded by the National Institute of Aging (NIA) (R01AG080981 to D.W., M.M.C., and J.G.; R01AG072743 to D.W.), the National Institute for Health and Care Research (NIHR) (R01NS102156 and R61NS115132 to M.M.C.).

Notes

The authors declare no competing financial interest.

■ ACKNOWLEDGMENTS

The authors acknowledge Dr. Tan from Sigma-Aldrich ISOTEC for assistance in synthesizing the 2-deoxy-D-glucose-2,2-d_2 enriched probe.

■ REFERENCES

(1) Kwon, H. W.; Becker, A.-K.; Goo, J. M.; Cheon, G. J. FDG Whole-Body PET/MRI in Oncology: A Systematic Review. *Nucl. Med. Mol. Imaging* **2017**, *51* (1), 22−31.
(2) Foster, N. L.; Heidebrink, J. L.; Clark, C. M.; Jagust, W. J.; Arnold, S. E.; Barbas, N. R.; DeCarli, C. S.; Turner, R. S.; Koeppe, R. A.; Higdon, R.; Minoshima, S. FDG-PET Improves Accuracy in Distinguishing Frontotemporal Dementia and Alzheimer's Disease. *Brain* **2007**, *130* (10), 2616−2635.
(3) Ahlman, M. A.; Grayson, P. C. Advanced Molecular Imaging in Large-Vessel Vasculitis: Adopting FDG-PET into a Clinical Workflow. *Best Pract. Res. Clin. Rheumatol.* **2023**, *37* (1), No. 101856.
(4) Diehl, P.; Leipert. Th. Deuteronen-Kernresonanzspektroskopie. *Helv. Chim. Acta* **1964**, *47* (2), 545−557.
(5) Polvoy, I.; Qin, H.; Flavell, R. R.; Gordon, J.; Viswanath, P.; Sriram, R.; Ohliger, M. A.; Wilson, D. M. Deuterium Metabolic Imaging-Rediscovery of a Spectroscopic Tool. *Metabolites* **2021**, *11* (9), 570.
(6) Chen Ming Low, J.; Wright, A. J.; Hesse, F.; Cao, J.; Brindle, K. M. Metabolic Imaging with Deuterium Labeled Substrates. *Prog. Nucl. Magn. Reson. Spectrosc.* **2023**, *134*−*135*, 39−51.
(7) Zhang, G.; Cullen, Q.; Berishaj, M.; Deh, K.; Kim, N.; Keshari, K. R. [6,6′-$^2H_2$] Fructose as a Deuterium Metabolic Imaging Probe in Liver Cancer. *NMR Biomed.* **2023**, *36* (10), No. e4989.
(8) Mahar, R.; Donabedian, P. L.; Merritt, M. E. HDO Production from [$^2H_7$]Glucose Quantitatively Identifies Warburg Metabolism. *Sci. Rep.* **2020**, *10* (1), 8885.
(9) Peters, D. C.; Markovic, S.; Bao, Q.; Preise, D.; Sasson, K.; Agemy, L.; Scherz, A.; Frydman, L. Improving Deuterium Metabolic Imaging (DMI) Signal-to-Noise Ratio by Spectroscopic Multi-Echo BSSFP: A Pancreatic Cancer Investigation. *Magn. Reson. Med.* **2021**, *86* (5), 2604−2617.
(10) Montrazi, E. T.; Bao, Q.; Martinho, R. P.; Peters, D. C.; Harris, T.; Sasson, K.; Agemy, L.; Scherz, A.; Frydman, L. Deuterium Imaging of the Warburg Effect at Sub-Millimolar Concentrations by Joint Processing of the Kinetic and Spectral Dimensions. *NMR Biomed.* **2023**, *36* (11), No. e4995.
(11) Miranda, A.; Glorie, D.; Bertoglio, D.; Vleugels, J.; De Bruyne, G.; Stroobants, S.; Staelens, S.; Verhaeghe, J. Awake 18F-FDG PET Imaging of Memantine-Induced Brain Activation and Test-Retest in Freely Running Mice. *J. Nucl. Med.* **2019**, *60* (6), 844−850.
(12) Shang, H.; Larson, P. E. Z.; Kerr, A.; Reed, G.; Sukumar, S.; Elkhaled, A.; Gordon, J. W.; Ohliger, M. A.; Pauly, J. M.; Lustig, M.; Vigneron, D. B. Multiband RF Pulses with Improved Performance via Convex Optimization. *J. Magn. Reson.* **2016**, *262*, 81−90.
(13) Skinner, J. G.; Topping, G. J.; Nagel, L.; Heid, I.; Hundshammer, C.; Grashei, M.; van Heijster, F. H. A.; Braren, R.; Schilling, F. Spectrally Selective BSSFP Using Off-Resonant RF Excitations Permits High Spatiotemporal Resolution 3D Metabolic Imaging of Hyperpolarized [1-^{13}C]Pyruvate-to-[1-^{13}C]Lactate Conversion. *Magn. Reson. Med.* **2023**, *90* (3), 894−909.
(14) Goldenberg, J. M.; Cárdenas-Rodríguez, J.; Pagel, M. D. Preliminary Results That Assess Metformin Treatment in a Preclinical Model of Pancreatic Cancer Using Simultaneous [^{18}F]FDG PET and AcidoCEST MRI. *Mol. Imaging Biol.* **2018**, *20* (4), 575−583.
(15) De Feyter, H. M.; Behar, K. L.; Corbin, Z. A.; Fulbright, R. K.; Brown, P. B.; McIntyre, S.; Nixon, T. W.; Rothman, D. L.; de Graaf, R. A. Deuterium Metabolic Imaging (DMI) for MRI-Based 3D Mapping of Metabolism in Vivo. *Sci. Adv.* **2018**, *4* (8), No. eaat7314.
(16) Straathof, M.; Meerwaldt, A. E.; De Feyter, H. M.; de Graaf, R. A.; Dijkhuizen, R. M. Deuterium Metabolic Imaging of the Healthy and Diseased Brain. *Neuroscience* **2021**, *474*, 94−99.
(17) Hargreaves, B. A. Rapid Gradient-Echo Imaging. *J. Magn. Reson. Imaging* **2012**, *36* (6), 1300−1313.
(18) Hartmann, B.; Müller, M.; Seyler, L.; Bäuerle, T.; Wilferth, T.; Avdievitch, N.; Ruhm, L.; Henning, A.; Lesiv, A.; Ivashkin, P.; Uder, M.; Nagel, A. M. Feasibility of Deuterium Magnetic Resonance Spectroscopy of 3-*O*-Methylglucose at 7 T. *PLoS One* **2021**, *16* (6), No. e0252935.
(19) Reivich, M.; Kuhl, D.; Wolf, A.; Greenberg, J.; Phelps, M.; Ido, T.; Casella, V.; Fowler, J.; Hoffman, E.; Alavi, A.; Som, P.; Sokoloff, L. The [18F]Fluorodeoxyglucose Method for the Measurement of Local Cerebral Glucose Utilization in Man. *Circ. Res.* **1979**, *44* (1), 127−137.
(20) Hess, S.; Blomberg, B. A.; Zhu, H. J.; Høilund-Carlsen, P. F.; Alavi, A. The Pivotal Role of FDG-PET/CT in Modern Medicine. *Acad. Radiol.* **2014**, *21* (2), 232−249.
(21) Simpson, R. J.; Brindle, K. M.; Brown, F. F.; Campbell, I. D.; Foxall, D. L. Studies of Pyruvate-Water Isotope Exchange Catalysed by Erythrocytes and Proteins. *Biochem. J.* **1981**, *193* (2), 401−406.
(22) Kotyk, J. J.; Rust, R. S.; Ackerman, J. J.; Deuel, R. K. Simultaneous in Vivo Monitoring of Cerebral Deoxyglucose and Deoxyglucose-6-Phosphate by ^{13}C[^{1}H] Nuclear Magnetic Resonances Spectroscopy. *J. Neurochem.* **1989**, *53* (5), 1620−1628.
(23) Raez, L. E.; Papadopoulos, K.; Ricart, A. D.; Chiorean, E. G.; Dipaola, R. S.; Stein, M. N.; Rocha Lima, C. M.; Schlesselman, J. J.; Tolba, K.; Langmuir, V. K.; Kroll, S.; Jung, D. T.; Kurtoglu, M.; Rosenblatt, J.; Lampidis, T. J. A Phase I Dose-Escalation Trial of 2-Deoxy-D-Glucose Alone or Combined with Docetaxel in Patients with Advanced Solid Tumors. *Cancer Chemother. Pharmacol.* **2013**, *71* (2), 523−530.
(24) Bhatt, A. N.; Shenoy, S.; Munjal, S.; Chinnadurai, V.; Agarwal, A.; Vinoth Kumar, A.; Shanavas, A.; Kanwar, R.; Chandna, S. 2-Deoxy-D-Glucose as an Adjunct to Standard of Care in the Medical Management of COVID-19: A Proof-of-Concept and Dose-Ranging Randomised Phase II Clinical Trial. *BMC Infect. Dis.* **2022**, *22* (1), 669.
(25) Singh, R.; Gupta, V.; Kumar, A.; Singh, K. 2-Deoxy-D-Glucose: A Novel Pharmacological Agent for Killing Hypoxic Tumor Cells, Oxygen Dependence-Lowering in COVID-19, and Other Pharmacological Activities. *Adv. Pharmacol. Pharm. Sci.* **2023**, *2023*, No. 9993386.
(26) Singh, D.; Banerji, A. K.; Dwarakanath, B. S.; Tripathi, R. P.; Gupta, J. P.; Mathew, T. L.; Ravindranath, T.; Jain, V. Optimizing Cancer Radiotherapy with 2-Deoxy-d-Glucose Dose Escalation

https://doi.org/10.1021/jacsau.4c00888
JACS Au 2025, 5, 571−577

Studies in Patients with Glioblastoma Multiforme. *Strahlenther. Onkol.* **2005**, *181* (8), 507−514.
(27) Nair, A. B.; Jacob, S. A Simple Practice Guide for Dose Conversion between Animals and Human. *J. Basic Clin. Pharm.* **2016**, *7* (2), 27−31.
(28) Brereton, I. M.; Irving, M. G.; Field, J.; Doddrell, D. M. Preliminary Studies on the Potential of in Vivo Deuterium NMR Spectroscopy. *Biochem. Biophys. Res. Commun.* **1986**, *137* (1), 579−584.
(29) Ackerman, J. J.; Ewy, C. S.; Becker, N. N.; Shalwitz, R. A. Deuterium Nuclear Magnetic Resonance Measurements of Blood Flow and Tissue Perfusion Employing 2H2O as a Freely Diffusible Tracer. *Proc. Natl. Acad. Sci. U. S. A.* **1987**, *84* (12), 4099−4102.
(30) Busch, R.; Neese, R. A.; Awada, M.; Hayes, G. M.; Hellerstein, M. K. Measurement of Cell Proliferation by Heavy Water Labeling. *Nat. Protoc.* **2007**, *2* (12), 3045−3057.
(31) Buxbaum, N. P.; Farthing, D. E.; Maglakelidze, N.; Lizak, M.; Merkle, H.; Carpenter, A. C.; Oliver, B. U.; Kapoor, V.; Castro, E.; Swan, G. A.; Dos Santos, L. M.; Bouladoux, N. J.; Bare, C. V.; Flomerfelt, F. A.; Eckhaus, M. A.; Telford, W. G.; Belkaid, Y.; Bosselut, R. J.; Gress, R. E. In Vivo Kinetics and Nonradioactive Imaging of Rapidly Proliferating Cells in Graft-versus-Host Disease. *JCI Insight* **2017**, *2* (12), No. e92851.
(32) Kushner, D. J.; Baker, A.; Dunstall, T. G. Pharmacological Uses and Perspectives of Heavy Water and Deuterated Compounds. *Can. J. Physiol. Pharmacol.* **1999**, *77* (2), 79−88.

https://doi.org/10.1021/jacsau.4c00888
JACS Au 2025, 5, 571−577